

Study of the ionic Peierls-Hubbard model using density matrix renormalization group methods

Y. Z. Zhang¹, C. Q. Wu², and H. Q. Lin³

¹*Max-Planck-Institut für Physik komplexer Systeme,
Nöthnitzer Straße 38 01187 Dresden, Germany*

²*Research Center for Theoretical Physics, Fudan University,
Shanghai 200433, China*

³*Department of Physics, The Chinese University of Hong Kong, Hong
Kong, China*

(October 6, 2018)

Density matrix renormalization group methods are used to investigate the quantum phase diagram of a one-dimensional half-filled ionic Peierls-Hubbard model at the antiadiabatic limit where quantum phonon fluctuations are taken into account partially. We found that two continuous phase transitions always exist from dimerized spin-gapped (bond-order-wave) state to band-insulator and undimerized spin-gapless (Mott-insulator) phase while undimerized spin-gapless phase vanishes at the adiabatic limit. Our results indicate that quantum phonon fluctuations, electron-electron interaction and ionic potential combine in the formation of the bond-order wave phase.

PACS: 71.30.+h; 71.10.Fd; 71.10.Pm

The response of correlated electrons to lattice distortions in solids has been extensively studied over the years, due to its important role in several classes of materials including high- T_c cuprates, colossal magnetoresistance manganites, conducting polymers and organic charge-transfer salts. As a good example, the Peierls-Hubbard model, with on-site Coulomb repulsion and lattice displacement, is a simple yet nontrivial model that exhibits a rich ground state phase diagram. Strong correlations lead to the separation of charge and spin excitations¹ while quantum phonon fluctuations can destroy an ordered gapped state²⁻⁴. Taking them both into consideration is essential for a full understanding of the nature of these materials.

With the inclusion of additional terms to the Peierls-Hubbard Hamiltonian on different physics background, various one-dimensional correlated electronic models were actively studied recently such as the ionic Peierls-Hubbard model⁵⁻⁸ which is defined as follows

$$\begin{aligned}
 H = & - \sum_l [t - \alpha (u_l - u_{l+1})] B_{l,l+1} + \Delta \sum_{l\sigma} (-1)^l n_{l\sigma} \\
 & + U \sum_l \left(n_{l\uparrow} - \frac{1}{2} \right) \left(n_{l\downarrow} - \frac{1}{2} \right) \\
 & + \frac{1}{2} K \sum_l (u_l - u_{l+1})^2 + \frac{1}{2M} \sum_l p_l^2, \quad (1)
 \end{aligned}$$

where $n_{l\sigma}$ is the number operator at site l , Δ is electrostatic potential of cations, and anions in charge-transfer salts, u_l (p_l) is the displacement (momentum) of the site l , α and K are the constant for the electron-phonon coupling and lattice elasticity, M is the mass and the bond-charge density operator $B_{l,l+1}$ is

$$B_{l,l+1} = \sum_{\sigma} \left(c_{l,\sigma}^{\dagger} c_{l+1,\sigma} + c_{l+1,\sigma}^{\dagger} c_{l,\sigma} \right). \quad (2)$$

Here we only considered half-filled case.

At $U = 0$, model (1) can be solved exactly at the adiabatic limit. In Appendix A, we give the detail process and discuss the definitions of the quantities we used below. Only one phase transition can be found from dimerized state which is also called Bond-Order-Wave (BOW) state to Band-Insulator (BI) phase as a function of electron-phonon (e-p) coupling strength. At $\Delta = 0$, it is well-known that no phase transition will occur even when U goes to infinity as long as there exists e-p coupling at the adiabatic limit. At $U \neq 0$ and $\Delta \neq 0$, earlier work^{5,6} and recent work^{7,8} which studied the e-p interaction only in the adiabatic limit also concluded that only one phase transition, i.e., from the BOW to the BI phase, will be present. In other words, the ionic phase with one electron per site is always dimerized. Therefore, the phase diagram of this model at the adiabatic limit is obvious. Only two phases, i.e. BOW and BI phase, can be detected.

When the lattice distortion is absent, Eq. (1) represents the Ionic Hubbard Model (IHM)⁹⁻¹⁵, which was used to describe the neutral-ionic phase transition in mixed-stack charge transfer crystals¹⁶⁻¹⁹. As pointed out by Fabrizio, Gogolin and Nersesyan⁹, there exists an unusual spontaneously dimerized insulator phase, the BOW phase, which separates the BI from the Mott insulator (MI) phase⁹. However, in reality, a lattice distortion always exists and it couples to electronic degrees of freedom strongly in these crystals. Structure changes, such as volume contraction could be used as an external parameter to drive the neutral-ionic transition¹⁸. Photoinduced cooperative phenomena were also observed¹⁹. So an important issue to address is the effect of electron-phonon interactions on the phase diagram.

However, it is well known that results obtained at the adiabatic limit are unreliable. For the Su-Schrieffer-Heeger (SSH) model, Fradkin and Hirsch²⁰ pointed out that the low-energy behavior of the system is actually governed by the antiadiabatic limit $M = 0$, rather than the adiabatic limit $M \rightarrow \infty$. The system at any non-zero frequency is renormalized to the limit of infinite frequency. For the Holstein model² and the spin-Peierls model³, more sophisticated calculations showed that uniform gapless phase exists unless the e-p coupling is sufficiently large. On the other hand, the system is found always in the dimerized gapped state at the adiabatic limit. Therefore, in order to study the effect of e-p interaction truly and understand the whole phase diagram, it is necessary to investigate the ground state properties of the system at the antiadiabatic limit.

In the present work, we perform an extensive numerical study of Eq. (1) at the antiadiabatic limit using the density matrix renormalization group (DMRG)²¹ technique. We found that, even with very strong e-p coupling, two continuous phase transitions from BI phase to MI phase are obtained from this model. One is the spin transition at $U = U_s$ where spin excitation gap closed, and the other is the charge transition at $U = U_c < U_s$ where the charge excitation gap vanishes. Between these two critical points, the system is dimerized. In contrast to the adiabatic limit where MI phase vanishes⁵⁻⁸, this means the ionic phase can also be undimerized after considering quantum phonon fluctuations. Our phase diagram is similar to that of IHM^{11,22} which is still highly controversial over the years⁹⁻¹⁵. Furthermore, in the region of strong ionic potential, the critical values U_c and U_s decrease simultaneously with increasing e-p coupling, while U_s will increase with increasing e-p coupling at sufficiently small ionic potential. The ground state phase diagram is obtained with the use of finite-size-scaling analysis.

At the antiadiabatic limit $M = 0$, an effective interacting fermion model²⁰

$$H = -t \sum_l B_{l,l+1} + U \sum_l \left(n_{l\uparrow} - \frac{1}{2} \right) \left(n_{l\downarrow} - \frac{1}{2} \right) - W \sum_l (B_{l,l+1})^2 + \Delta \sum_{l\sigma} (-1)^l n_{l\sigma}, \quad (3)$$

can be obtained where the effective bond-charge attraction ($W \equiv \alpha^2/2K$) term accounts for the contribution of the phonon quantum fluctuations. So the Hamiltonian (3) could be viewed as a 1D e-p interacting system including both the quantum phonon fluctuations and the electron correlations.

In this paper, we have applied the finite-size DMRG algorithm with open boundary conditions to study the Hamiltonian (3) at half-filling. This method allows us to probe directly correlation functions and structure factors associated with the spin density wave (SDW), the charge density wave (CDW) and the bond order wave in the ground state. Lattices up to 512 sites were frequently used in our studies. The largest number of states kept

in the calculation was $m = 512$ per block. The hopping integral t is set to 1 as the energy unit. The weight of the discarded states was typically about $10^{-7} - 10^{-10}$ depending on whether the system is in its critical state or not in the final sweep. The convergence tests as functions of number of states kept were carefully performed. We checked our DMRG calculations against exact numerical results for noninteracting ($U = W = 0$) chains (up to 512 sites) and results from exact diagonalization for interacting ($U \neq 0, W \neq 0$) chains (up to 14 sites). Excellent agreement was found in both cases. When interactions are turned on, there exist finite excitation gaps on finite chains, so the accuracies of all quantities we calculated are no worse than that of the noninteracting case. Thus, numerical errors in our work could be safely estimated to be smaller than 10^{-4} .

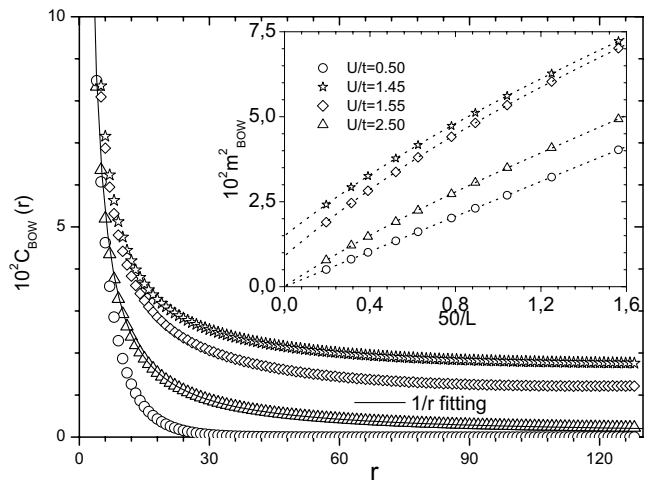


FIG. 1. The staggered BOW correlation functions of the ionic Peierls-Hubbard model for $\Delta/t = 0.30$ and $W/t = 0.30$. The inset shows an extrapolation of $m_{BOW}^2(L)$ with a third-order polynomial in $1/L$.

Now let's introduce a way to determine the phase boundaries accurately. Although parts of this method have already been first used in determining the phase boundaries of IHM¹², we perform this method more carefully and systematically in this paper than ever by using various finite-size analysis. First we defined the staggered BOW correlation function which is the most direct evidence for the long-range BOW state

$$C_{BOW}(r) = (-1)^r \left(\frac{1}{L_{av}} \sum_l \langle B_{l,l+1} B_{l+r,l+r+1} \rangle - \bar{B}^2 \right) \quad (4)$$

where $\bar{B} = \frac{1}{L} \sum_l \langle B_{l,l+1} \rangle$. In Fig. 1, we show the staggered BOW correlation functions with increasing Hubbard U at $\Delta/t = 0.30$ and $W/t = 0.30$. Here we only perform the average in eq. (4) over 256 sites in the middle of the 512-site system, i.e. the sum over l is from 129

to 256 and $L_{av} = 128$, in order to further avoid boundary effects. L is the half of the chain length N which is located in the central of the system to further eliminate edge effects. The results indicate that there exist three different phases in model (3) since the staggered BOW correlation functions show three distinct type of behavior as r increases: (i) it decays exponentially at $U/t = 0.50$, indicating that the system has no BOW order; (ii) it converges to a nonzero constant at $U/t = 1.45$ and $U/t = 1.55$, indicating that the system is in the BOW phase with a finite width; (iii) it decays as $1/r$ at $U/t = 2.50$, indicating that the system is in another phase. The BOW order parameter in the thermodynamic limit

$$\Delta_{BOW} = \lim_{L \rightarrow \infty} \frac{1}{L} \sum_l (-1)^{l+1} \langle B_{l,l+1} \rangle \quad (5)$$

can be obtained by fitting $m_{BOW}^2(L) (= \frac{1}{L} \sum_r C_{BOW}(r))$, where the sum over r goes to L) with a third-order polynomial in $1/L$ since $m_{BOW}^2(L) \rightarrow \Delta_{BOW}^2$ for $L \rightarrow \infty$. The inset of Fig. 1 shows such extrapolations. In the following we always take $L_{av} = 4$ which is enough to minimize the oscillations due to the open boundary conditions and sum over r is only take over central L site where L is half of the chain length N to further eliminate edge effects. We find that $m_{BOW}^2(L)$ approaches zero when $U/t = 0.50$ and 2.50 but remains finite when $U/t = 1.45$ and $U/t = 1.55$ which indicate that there exists a finite region of the BOW phase.

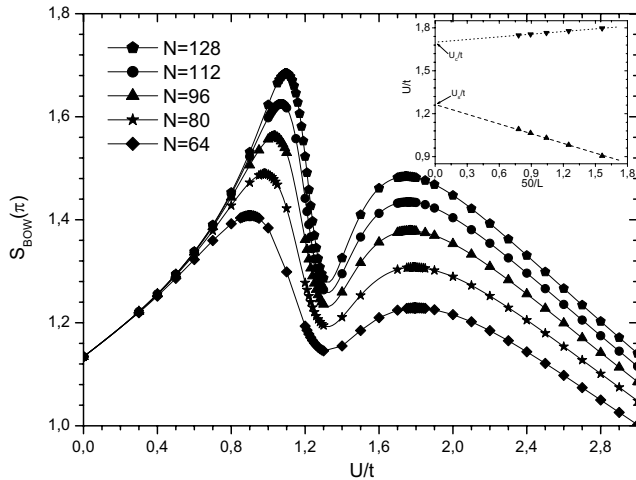


FIG. 2. Behavior of $S_{BOW}(\pi)$ across the phase boundary for $\Delta/t = 0.3$, $W/t = 0.30$. The inset shows a linear extrapolation of the critical values U_c and U_s with $1/L$.

Next we have studied the nature of BI-BOW and BOW-MI transitions by calculating the static structure factors corresponding to different phases to determine the phase boundaries. The first structure factor studied is

$$S_{BOW}(q) = \frac{1}{L_{av}} \sum_{lr} e^{iqr} (\langle B_{l,l+1} B_{l+r,l+r+1} \rangle)$$

$$- \langle B_{l,l+1} \rangle \langle B_{l+r,l+r+1} \rangle. \quad (6)$$

According to Fabrizio et. al.⁹, phase transitions on the BI-BOW and BOW-MI phase boundaries are an Ising type and KT type respectively, the staggered connected correlation function falls off algebraically as

$$(-1)^r (\langle B_{l,l+1} B_{l+r,l+r+1} \rangle - \langle B_{l,l+1} \rangle \langle B_{l+r,l+r+1} \rangle) \sim r^{-\eta} \quad (7)$$

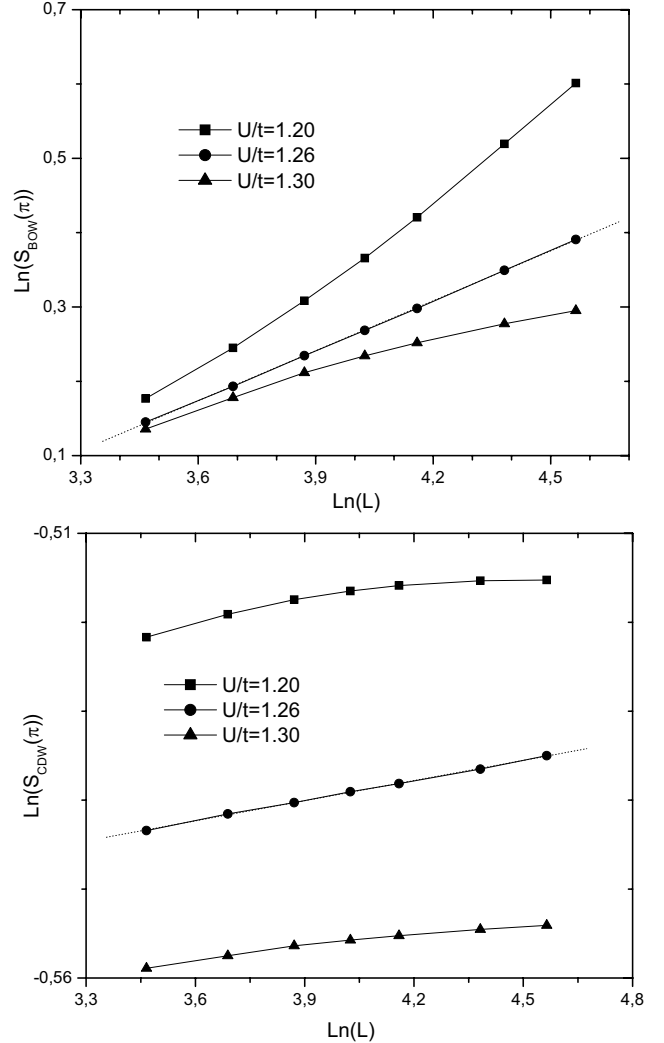


FIG. 3. Finite-size analysis for $S_{BOW}(\pi)$ and $S_{CDW}(\pi)$ in the vicinity of the first phase transition at U_c for $\Delta/t = 0.30$, $W/t = 0.30$.

Away from phase boundaries, this quantity falls off exponentially. Therefore the $S_{BOW}(\pi)$ is expected to diverge at these two critical points if $\eta \leq 1$ or reach maximums if $\eta > 1$ as the system size goes to infinity. Fig. 2 shows the results of the $S_{BOW}(\pi)$ for different system

sizes with $\Delta/t = 0.30$, $W/t = 0.30$ and $0 < U/t < 3$. As expected, the $S_{BOW}(\pi)$ peaks twice for all the different system sizes we calculated. The positions of these two peaks become closer as the system size is larger. The inset of Fig. 2 shows linear extrapolations of the positions of these two peaks with $1/L$. We find that these two peaks will not merge at $L \rightarrow \infty$ which indicate again that the BOW phase remains finite at thermodynamic limit. In order to give more convincing evidence, we did another finite-size analysis in the vicinity of these two phase transitions. Let us start from the first phase transition at $U = U_c$. Fig. 3(a) presents plots of $\ln[S_{BOW}(\pi)]$ versus $\ln[L]$ for $\Delta/t = 0.30$, $W/t = 0.30$ and three different values of U/t around the first critical point. Data points for $U/t = 1.26$ indeed fall on a straight line, indicating critical scaling for the BOW fluctuations. At the other two points $U/t = 1.20$ and 1.30 , data points behave nonlinearly due to the exponential decay term. Applying the same finite-size analysis to the CDW structure factor $S_{CDW}(\pi)$, we can also explore the nature of the first phase transition. The CDW structure factor is defined as

$$S_{CDW}(q) = \frac{1}{L_{av}} \sum_{lr} e^{iqr} (\langle n_l n_{l+r} \rangle - \langle n_l \rangle \langle n_{l+r} \rangle) \quad (8)$$

The linear behavior of $\ln[S_{CDW}(\pi)]$ around $U/t = 1.26$, shown in Fig. 3(b), confirms the vanishing of the charge gap at the first phase transition point.

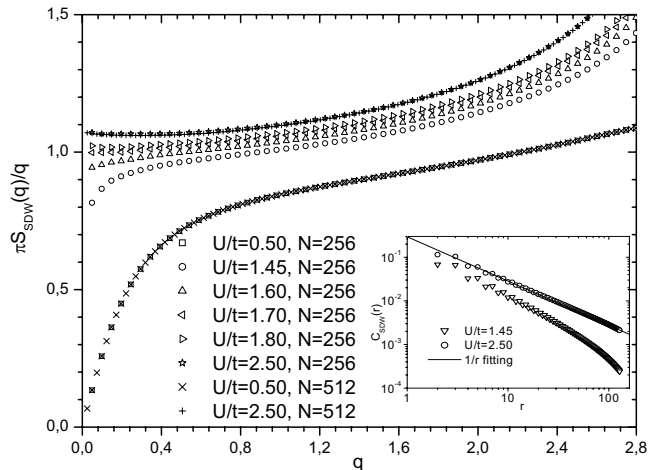


FIG. 4. $\pi S_{SDW}(q)/q$ vs q for $\Delta/t = 0.30$, $W/t = 0.30$ and 6 different values of U across the MI-BOW boundary.

Next we determine the nature of the second phase transition at $U = U_s$. As predicted by Fabrizio et. al.⁹, it is a quantum phase transition of the KT type. This makes it difficult to determine the phase boundary directly from the behavior of $S_{BOW}(\pi)$ and $S_{SDW}(\pi)$ (defined below) due to the finite-size effects. Instead, we apply an indirect method, used by Sengupta et al.⁴, to confirm the second phase transition. The SDW structure factor is defined as

$$S_{SDW}(q) = \frac{1}{L_{av}} \sum_{lr} e^{iqr} \langle s_l^z s_{l+r}^z \rangle. \quad (9)$$

It is well known²³ that if the ground state of a 1D system is spin-gapless, the spin-spin correlation falls algebraically with exponent equal to 1. It has been further shown²⁴ that in the spin-gapless phase $S_{SDW}(q)/q \rightarrow 1/\pi$ as $q \rightarrow 0$ whereas in the spin-gapped phase $S_{SDW}(q)/q \rightarrow 0$. Even a very small spin gap can be detected in this way, since it is in practice sufficient to see the $\pi S_{SDW}(q)/q$ decay below 1 for small q to conclude that a spin gap must be present. Fig. 4 shows the behavior of $\pi S_{SDW}(q)/q$ for $\Delta/t = 0.30$, $W/t = 0.30$ and different values of U/t . In the gapless region, logarithmic corrections²⁵ make it difficult to observe the approach to 1 as $q \rightarrow 0$. In analogy with spin systems²⁶, we expect the leading logarithmic corrections to vanish at the point where spin gap opens and therefore exactly at the critical point there should be a clear scaling to 1. Based on results shown in Fig. 4, we estimate the MI-BOW boundary to be at $U/t = 1.70 \pm 0.02$ at $\Delta/t = 0.30$, $W/t = 0.3$ which is consistent with the results shown in Fig. 2. The inset of Fig.4 further provides evidence for the transition from the spin-gapped state, as identified by the exponential decay of the staggered SDW correlation function, to the spin-gapless state, as characterized by the $1/r$ -decay of the SDW correlation function.

$$C_{SDW}(r) = \frac{1}{L} (-1)^r \sum_l \langle s_l^z s_{l+r}^z \rangle \quad (10)$$

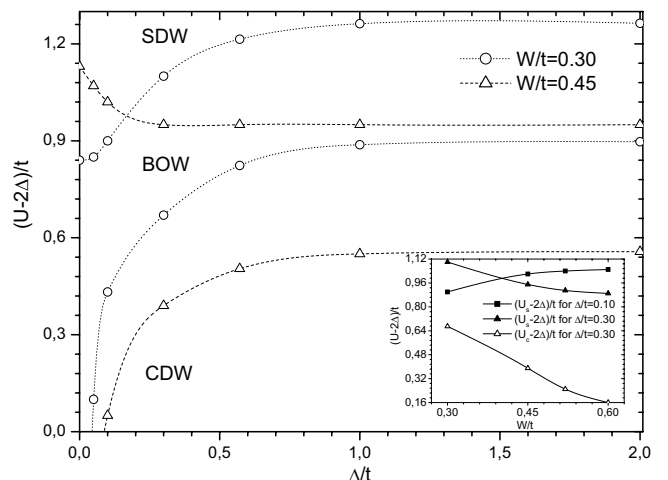


FIG. 5. Phase diagram of model (3) for two different e-p couplings. The inset shows different behavior of U_s for weak ($\Delta/t = 0.10$) and strong ($\Delta/t = 0.30$) ionic potentials as a function of e-p coupling W . While the behavior of U_c as a function of W is always the same for all ionic potentials. Here we only show the plot for U_c at $\Delta/t = 0.30$.

Finally, we present in Fig. 5 the resulting phase diagram in the $U - \Delta$ plane for two values of W . For $\Delta = U = 0$, model (3) becomes the $t - W$ model²⁷ which can be mapped from the SSH model at the antiadiabatic limit. This model has been studied by the DMRG method²⁷ and the renormalization group analysis²⁰. The ground state is dimerized and the BOW order parameter is nonvanishing as long as $W \neq 0$. After switching on the Hubbard U or a finite ionic potential Δ , the BOW phase could be destroyed. The model undergoes quantum phase transitions from the BOW phase either to the MI phase or the BI phase. The critical value U and Δ will increase with increasing e-p coupling W . In the weak ionic potential region, such as $\Delta/t = 0.1$, on increasing the e-p coupling W , the transition points U_c and U_s move apart and the separation between U_c and U_s becomes significantly larger. However, for strong ionic potential, such as $\Delta/t = 1.0$, both U_c and U_s decrease and the width of the BOW phase increases slightly with increasing e-p coupling. When the ionic potential is intermediate, such as $\Delta/t = 0.3$, U_c and U_s will also decrease simultaneously while the width of the BOW phase increases significantly. For model (1) at the adiabatic limit, a spin gap will always be present⁸. However, at the antiadiabatic limit, the transition from BOW to MI phase always occurs even though the e-p coupling is sufficiently large.

The inset of Fig. 5 shows the asymptotic behavior of the critical points U_c and U_s at $\Delta/t = 0.10$ and

$\Delta/t = 0.30$ with increasing e-p coupling. For weak on-site potential such as $\Delta/t = 0.10$, the critical point U_s becomes larger with increasing e-p coupling while for strong on-site potential for example $\Delta/t = 0.30$, it decrease monotonously with the increasing e-p coupling. However the behavior of U_c is the same for all value of on-site potential, it decreases monotonously as a function of e-p coupling. Here we only show one set of data at $\Delta/t = 0.30$.

In conclusion, we have studied 1D half-filled Ionic Peierls-Hubbard model at the antiadiabatic limit using the DMRG method. The phase diagram is obtained by investigating correlation functions and structure factors. In contrast to the adiabatic limit, the transition from the dimerized spin-gapped state to the spin-gapless state occurs for any value of the ionic potential Δ . Compared to the IHM, the BOW phase always exists in the presence of e-p coupling W . The first critical value U_c for the charge gap always decreases with increasing W while the second critical value U_s for the spin gap shows different behavior for weak and strong ionic potential.

It is a pleasure to acknowledge helpful discussions with Y. J. Wang, Y. L. Liu and P. Thalmeier, X. Q. Wang. This work is supported by the Research Grants Council of the HKSAR, Project No. CUHK 4037/02P. C. Q. Wu also acknowledges financial support from the National Natural Science Foundation of China (No. 19725414 and No. 90103034).

APPENDIX A: EXACT SOLUTION TO MODEL (1) AT THE ADIABATIC LIMIT IN THE NONINTERACTING CASE

In this appendix we solve model (1) exactly at the adiabatic limit in the noninteracting case. First we define the dimensionless coupling constant as $\lambda = 2\alpha^2/Kt$ and dimerized order parameter as $\delta = \alpha u/t$ where $(-1)^l u = u_l - u_{l+1}$. Then model (1) can be rewritten as following

$$H/t = - \sum_l \left[1 - (-1)^l \delta \right] B_{l,l+1} + D \sum_{l\sigma} (-1)^l n_{l\sigma} + \frac{1}{\lambda} \sum_l \delta^2 \quad (\text{A1})$$

where $D = \Delta/t$. Using Fourier transformation and unitary transformation, the original operator $c_{l\sigma}^+$ can be expressed as

$$c_{l\sigma}^+ = \frac{1}{\sqrt{N}} \sum_k e^{ikl} (\alpha_k^*(l) a_{k\sigma}^+ + \beta_k^*(l) b_{k\sigma}^+) \quad (\text{A2})$$

where

$$\alpha_k(l) = u_k + (-1)^l v_k, \beta_k(l) = -v_k^* + (-1)^l u_k \quad (\text{A3})$$

and $k \in (-\frac{\pi}{2}, \frac{\pi}{2}]$. Here

$$u_k = \frac{\sqrt{E_k - 2 \cos k}}{\sqrt{2E_k}}, v_k = \frac{-2i\delta \sin k}{\sqrt{2E_k(E_k - 2 \cos k)}} \quad (\text{A4})$$

where

$$E_k = \sqrt{4 \cos^2 k + 4\delta^2 \sin^2 k + D^2}. \quad (\text{A5})$$

Then the Hamiltonian (A1) can be diagonalized as

$$H/t = \sum_{k\sigma} E_k (a_{k\sigma}^+ a_{k\sigma} - b_{k\sigma}^+ b_{k\sigma}). \quad (\text{A6})$$

The quantities related to the BOW phase can be expressed as following

$$\langle B_{l+r, l+r+1} \rangle = 4 \left(A_1 - (-1)^{l+r} B_1 \right). \quad (\text{A7})$$

here B_1 is the order parameter, A_1 is the average bond length and

$$\begin{aligned} \langle B_{l+r, l+r+1} B_{l, l+1} \rangle &= \langle B_{l+r, l+r+1} \rangle \langle B_{l, l+1} \rangle + \\ &\left\{ \begin{array}{l} 4 \left[C_r^2 - (A_{r+1} - (-1)^l B_{r+1}) (A_{r-1} + (-1)^l B_{r-1}) \right], r = \text{even} \\ 4 [C_{r+1} C_{r-1} - (A_r^2 - B_r^2)], r = \text{odd} \end{array} \right\}. \end{aligned} \quad (\text{A8})$$

where

$$A_r = \frac{1}{\pi} \int_0^{\frac{\pi}{2}} dk \frac{2 \cos kr \cos k}{E_k}. \quad (\text{A9})$$

$$B_r = \frac{\delta}{\pi} \int_0^{\frac{\pi}{2}} dk \frac{2 \sin kr \sin k}{E_k}. \quad (\text{A10})$$

$$C_r = \frac{D}{\pi} \int_0^{\frac{\pi}{2}} dk \frac{\cos k}{E_k}. \quad (\text{A11})$$

Then we find that the definition (4), (5), and (6) in our paper is usefull. Since $\overline{B} = \frac{1}{L} \sum_l \langle B_{l, l+1} \rangle = 4A_1$, we can obtain

$$\begin{aligned} C_{BOW}(r) &= 16B_1^2 + \\ &\left\{ \begin{array}{l} 4 [C_r^2 - (A_{r+1} A_{r-1} + B_{r+1} B_{r-1})], r = \text{even} \\ 4 [(A_r^2 - B_r^2) - C_{r+1} C_{r-1}], r = \text{odd} \end{array} \right\}. \end{aligned} \quad (\text{A12})$$

Obviously, if the system is in the BOW phase, $C_{BOW}(r) \rightarrow 16B_1^2$ remains constant at large r otherwise $C_{BOW}(r) \rightarrow 0$ in the CDW phase since second line in eq. (A12) is exponential decay with the distance r in both phases. The BOW order parameter defined in our paper can be obtained as

$$\Delta_{BOW} = \lim_{L \rightarrow \infty} \frac{1}{L} \sum_l (-1)^{l+1} \langle B_{l, l+1} \rangle = 4B_1. \quad (\text{A13})$$

Meanwhile

$$m_{BOW}^2(\infty) = \lim_{L \rightarrow \infty} \frac{1}{L} \sum_r C_{BOW}(r) = 16B_1^2 \quad (\text{A14})$$

since the second line in eq. (A12) is exponential decay with the distance r . Here we should mention that on the phase boundary the second line in eq. (A12) is power-law decay. Nevertheless eq. (A14) is still valid. The staggered BOW structure factor is

$$S_{BOW}(\pi) = \left\{ \begin{array}{l} 4 [C_r^2 - (A_{r+1} A_{r-1} + B_{r+1} B_{r-1})], r = \text{even} \\ 4 [(A_r^2 - B_r^2) - C_{r+1} C_{r-1}], r = \text{odd} \end{array} \right\}. \quad (\text{A15})$$

As we mentioned above, exactly on the phase boundary it is power-law decay otherwise exponential decay. Finally we give the self-consistent equation which can be used to determine the phase diagram in the $\Delta - \lambda$ plane

$$1 = \frac{2\lambda}{\pi} \int_0^{\frac{\pi}{2}} dk \frac{2 \sin kr \sin k}{E_k}. \quad (\text{A16})$$

-
- ¹ V. J. Emery, in *Highly Conducting One-Dimensional Solids*, edited by J. T. Devreese, R. Evrand, and V. van Doren (Plenum, New York, 1979), p.327.
- ² C. Q. Wu, Q. F. Huang and X. Sun, Phys. Rev. B 52, 15683 (1995).
- ³ R. J. Bursill, R. H. McKenzie and C. J. Hamer, Phys. Rev. Lett. 83, 408 (1999).
- ⁴ P. Sengupta, A. W. Sandvik and D. K. Campbell, Phys. Rev. B 67, 245103 (2003).
- ⁵ N. Nagaosa, J. Phys. Soc. Jpn., **55**, 2754 (1986)
- ⁶ A. Painelli and A. Girlando, Phys. Rev. B 37, 5748 (1988) and reference therein.
- ⁷ S. Caprara, M. Avignon and O. Navarro, Phys. Rev. B 61, 15667 (2000).
- ⁸ L. D. Freo, A. Painelli and Z. G. Soos, Phys. Rev. Lett. 89, 27402 (2002) and reference therein.
- ⁹ M. Fabrizio, A. O. Gogolin and A. A. Nersesyan, Phys. Rev. Lett. 83, 2014 (1999).
- ¹⁰ T. Wilkens and R. M. Martin, Phys. Rev. B 63, 235108 (2001).
- ¹¹ M. E. Torio, A. A. Aligia and H. A. Ceccatto, Phys. Rev. B 64, 121105 (2001).
- ¹² Y. Z. Zhang, C. Q. Wu and H. Q. Lin, Phys. Rev. B 67, 205109 (2003).
- ¹³ J. Lou, S. Qin, T. Xiang, C. Chen, G. S. Tian and Z. B. Su, Phys. Rev. B 68, 045110 (2003).
- ¹⁴ P. Brune, G. I. Japaridze, A. P. Kampf and M. Sekania, cond-mat/0304697.
- ¹⁵ S. R. Manmana, V. Meden, R. M. Noack and K. Schoenhammer, cond-mat/0307741.
- ¹⁶ J. B. Torrance, et al., Phys. Rev. Lett. 46, 253 (1981); 47, 1747 (1981).
- ¹⁷ S. Horiuchi, et al., Phys. Rev. Lett. 85, 5210 (2000).
- ¹⁸ S. Horiuchi, et al., Science 299, 229 (2003).
- ¹⁹ E. Collet, et al., Science 300, 612 (2003).
- ²⁰ E. Fradkin and J. E. Hirsch, Phys. Rev. B 27, 1680 (1983).
- ²¹ S.R. White, Phys. Rev. B **48**, 10345 (1993).
- ²² For the IHM, the region of BOW phase is so small that it was argued for its existence in the literature. With the bond charge attraction term, the BOW region is much larger and we can distinguish the two phase transitions clearly. We regard this as an indirect confirmation of the BOW phase in the IHM.
- ²³ J. Voit, Rep. Prog. Phys. 58, 977 (1995); Phys. Rev. B 45, 4027 (1992).
- ²⁴ R. T. Clay, A. W. Sandvik and D. K. Campbell, Phys. Rev. B 59, 4665 (1999).
- ²⁵ S. Eggert, I. Affleck and M. Takahashi, Phys. Rev. Lett. 73, 332 (1994).
- ²⁶ S. Eggert, Phys. Rev. B 54, 9612 (1996).
- ²⁷ Y. Z. Zhang, C. Q. Wu and H. Q. Lin, Phys. Rev. B 66, 35115 (2002).